EXPERIMENTAL EVALUATION OF HIERARCHICAL FUNCTIONALLY GRADED LATTICES USING DIGITAL IMAGE CORRELATION AND MICRO-CT

Junyang Ye*, Ata Babazadeh-Naseri*, Benjamin J. Fregly*, C. Fred Higgs III*

*Department of Mechanical Engineering, Rice University, Houston, TX 77005

Abstract

Hierarchical meta-materials based on functionally-graded lattices (FGLs) have the benefit of customizable material properties. However, the effects of sharp transitions on the effective properties of FGLs have yet to be evaluated. This experimental study focused on characterizing the compressive properties of hierarchical FGLs built with smooth or sharp gradings. A total of 12 samples were 3D-printed in Ti-6Al-4V alloy and tested in axial compressive loading. Digital image correlation (DIC) was used to measure displacements and deformations. The 3D-printing quality of FGLs was also evaluated by micro-CT imaging of 5 samples. The results showed that the cross-sectional areas of struts in FGLs with sharp transitions were 26% smaller than uniform lattices and FGLs with smooth transitions. Compression testing also confirmed a lower average elastic modulus in FGLs with sharp gradings. These results will provide insights for incorporating adjustment factors to account for the loss of strength in FGLs.

Keywords: Hierarchical lattices, Manufacturing defects, Digital image correlation, Experimental, Functional graded lattice, Micro-CT, Ti-6Al-4V

Introduction

Recent development in metal additive manufacturing (MAM) has extended its application to wider fields including biomedical devices for its ability to fine-tune material properties on a macro scale [1]. In particular, MAM with selective laser melting (SLM) is well suited for producing bone implants, as the printed part can mimic human bone characteristics better than solid material [2]. These human bone characteristics include graded inner structure [3] and anisotropy [4]. While 3D-printed porous metals can in theory create anisotropy, it is still hard to fine-tune the degree of anisotropy while matching bone properties. Additionally, additively manufactured implants can create rough surfaces at the bone-implant interface to facilitate bone ingrowth and fixation, producing better osseointegration results [5]. To design implants that better match natural human bones, numerous studies have tried to utilize hierarchical lattice structures made of Ti-6Al-4V (Ti64) powder because of their high freedom in tuning unit cell size and solid volume fraction (or relative density), making a variety of applications possible [6–9]. However, it is not clear how precise is MAM in producing desired material properties at the meso-scale reliably. Deviation in as-built products from the original design can significantly alter the effective material property, rendering one of the biggest benefits of additive manufactured implants moot. Furthermore, since SLM uses metal powder as raw material, important material properties such as the equivalent Young's modulus compared to conventional solid material and subtractive manufacturing is still being studied [10]. Without such parameters, computational modeling will also be inaccurate in predicting the behavior of the implant. Therefore, it is necessary to perform experimental testing on SLM manufactured functionally graded lattices (FGL) to determine both the printing quality and product performance.

Most research regarding experimentally determining the properties of hierarchical lattices involved one-directional grading, meaning that the volume fraction of the samples either simply increase or decrease along the direction of grading [12] – [16]. Few have designed samples that use more complicated grading and resemble Voigt's iso-strain and Reuss's iso-stress conditions, which adds more possibilities in tailoring the hierarchical building blocks to meet specific needs. Onal et al. [16] used multiple ways to weigh the graded lattice samples to calculate the as-built volume fraction. While weighing the samples is a popular method, it cannot give much useful information about relative printing quality when the relative density is the same but the building blocks are

arranged differently. Scanning electron microscope (SEM) can produce high-resolution images of the surface condition of lattice samples, and has also been a popular choice in determining printing quality [15], [16], [18] – [20], but SEM can only observe the outmost struts of the lattices without knowing the conditions of internal struts. Few studies have compared printing quality and mechanical properties for hierarchical lattice samples that have the same volume fraction but different building block combinations and therefore, different gradings.

Micro Computer Tomography (micro-CT) is another popular way of examining printing quality, but most studies only analyze a selection of micro-CT slices and look for defects [18,20] only for qualitative analyses. In fact, micro-CT slices have the potential to be three dimensional reconstructed and analyzed in more quantitative methods [21]. Being able to access the 3D models of individual struts is crucial in comparing samples of the same volume fraction because weight measurements cannot provide insights in the manufacturing differences between samples if the weights do not match. It is often challenging to differentiate the differences originated from a consistent trend of misprinting certain grading patterns or simply more attached powders on lattice struts. Furthermore, struts are not necessarily printed to be perfectly circular in their cross sections. In this case, only the 3D view can provide more accurate measurements of the strut cross-sectional areas.

In this study we investigate and compare the mechanical properties and manufacturing-induced defects for samples of the same volume fraction and hierarchical building blocks but different gradings and loading directions through compression testing and micro-CT imaging. The functional grading used in this study is density-varying discrete unit cell grading for truss-based lattices achieved by stacking unit cells of different strut diameters together. We seek to combine the mechanical testing results and micro-CT measurements of strut cross-sectional areas to explain the effects of manufacturing process caused by the discontinuities of different severity in discrete unit cell grading on the mechanical performance of lattice structures. A total of 12 compression samples and five micro-CT samples were manufactured and tested from Ti64 powder using SLM with building blocks that have relative densities ranging between 37% and 79%. The mechanical testing results were post-processed with Digital Image Correlation (DIC) to obtain true stress-strain curves, stiffness, yield stress and yield strain. Three types of struts, uniform struts, struts shared in smooth grading and struts shared in sharp grading, were reconstructed and measured from micro-CT samples.
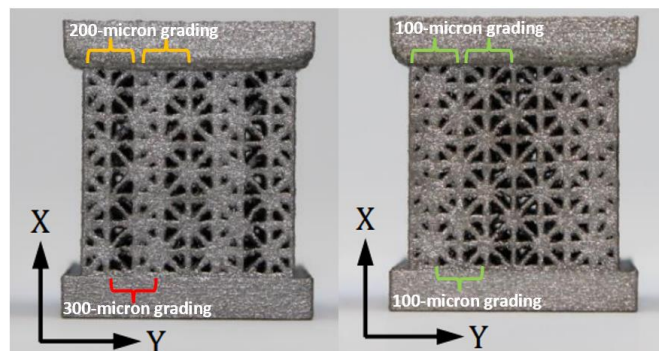
Methods

Mechanical testing

Functionally graded lattice (FGL) structures were designed and manufactured for testing using the hierarchical design process. Body Diagonal-Face Diagonal Cubic (BD-FDC) unit cells, according to the naming convention presented by Shi and Akbarzadeh [22], were selected as building blocks for assembling 2nd order hierarchical lattice structures. Each unit cell in the assembly took one out of four possible orientations and had a strut diameter assigned from four sizes ranging from 300 μm to 600 μm that corresponded to four different solid volume fractions from 37% to 79% for each sample (**Fig. 1**). With different combinations of a total of 16 available types of building blocks (four unit cell types, four relative densities), functional grading of the lattice structure was achieved. A more detailed description of the hierarchical design process will be communicated in a separate publication.

Two sets of FGLs were investigated: lattice structures with smooth (or linear) grading and lattice structures with sharp transitions (or nonlinear grading). For smooth grading, layers of unit cells with different relative densities had maximum strut diameter differences of 100 μm, while for sharp grading, the strut diameter differences ranged between 200 and 300 μm (**Fig. 2**). For clarity, linearly graded lattice bodies with smooth transitions are herein referred to as L lattices whereas sharply graded lattice bodies are herein referred to as S lattices throughout the paper. Note that the linear grading in this study also refers to stacking unit cells of discrete linear strut diameter difference, similar to some of the previous studies [23–25], while sharp grading does not follow the linear step-wise strut diameter difference pattern. All lattice structures were graded in the same y-direction, but they were tested in two directions to examine the anisotropy of the FGL. Two solid blocks were

added to the top and bottom of the lattice structure in direction of intended loading, which could be either x or y-direction.
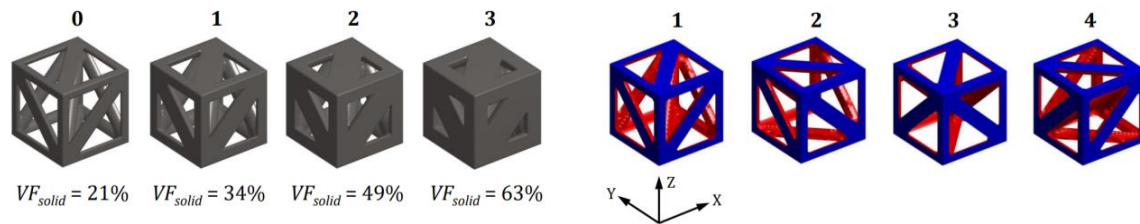
Fig. 1. Proposed hierarchical building blocks of four unit cell orientation types and four relative densities (or solid volume fraction, VF_{solid}).


Fig. 2. Left: Type S lattice with 200-micron and 300-micron thickness difference grading. Right: Type L lattice with 100-micron thickness difference grading. Both shown in X-loading direction.

Following the methodology of lattice grading described above, a total of 12 compression samples were designed and manufactured (**Fig. 3**). This included 3 samples in each of the four categories (x-direction type L, x-direction type S, y-direction type L, y-direction type S). The lattice bodies of the compression samples were cubic and contained 8 unit cells with a side length of 1.5 mm in each direction, thus having side lengths of 12 mm. Top and bottom square plates with side lengths of 14 mm and thicknesses of 2.5 mm were added to the compression samples to ensure even contact when testing. Top plates were engraved with batch numbers for easy identification. Lattices loaded in x-direction were intended to resemble Voigt's iso-strain conditions, while lattices loaded in y-direction were designed to resemble Reuss's iso-stress condition. In each group of samples of the iso-strain or iso-stress condition, three samples had sharp grading and the other three had smooth grading. The lattice structures were designed using an implicit geometry modeling framework developed in MATLAB (*MathWorks, Natick, MA, USA*) and nTop (*nTopology, New York City, NY, USA*). The final designs were sent to 3D Systems' on-demand manufacturing services (*Rock Hill, SC, USA*) for manufacturing with Ti64 alloy powder using Direct Metal Printing (DMP), an SLM process. Ti-6Al-4V Grade 23 powder was used as a raw material with a layer thickness of 30 μm. The samples were heat-treated and electrical discharge machining (EDM) processed to a surface roughness value of Ra = 2-4 μm.

Compression testing was carried out on an MTS 810 machine with a maximum of 200 kips compression force and data was gathered using the MTS 793 MultiPurpose TestWare software. A metal block was placed above the samples to protect the MTS machine by preventing excessive stress that could cause the deformation of the contact surface due to the small surface area of the samples. A total of 12 compression tests were performed with one test per sample, and the loading rate was set to 0.5 mm/min in all tests. All samples were loaded monotonically until significant structural failures were observed, or displacements exceeded 6 mm. The applied force was measured via a 200-kips load cell and displacements were recorded using the internal displacement transducer of the hydraulic jack. The entire testing process was recorded on a cell phone camera (12 MP sensor, 77mm equivalent f/2.8-aperture). Testing of three samples were also recorded on an Olympus TG6 camera (12

MP sensor, 35mm equivalent f/2.0-aperture). Data gathered from the MTS machine was processed using an in-house MATLAB code. For each sample, the maximum slope in the elastic region was found to represent elastic stiffness. The force-displacement response of each sample was normalized, and stress-strain curve (engineering and true) were calculated. The 0.2% offset method was used to find the corresponding yield strength for each sample.

Video recordings that were deemed suitable (9 of the 12) were used for Digital Image Correlation (DIC) processing to directly measure the deformation of the lattice structure at the one frame per second rate. One video for sharply graded y-direction sample and two videos for linearly graded y-direction samples were not successful in DIC processing due to improper focus of the image. Pixel size for each footage was calibrated based on calibration patterns that were placed around the sample before starting the test. An opensource implementation of 2D Finite Element Global Digital Image Correlation (FE-DIC) in MATLAB [26] was used for DIC processing, and in-house MATLAB code was utilized for estimating the DIC-adjusted loading rate only for the lattice structure, excluding other deforming components.
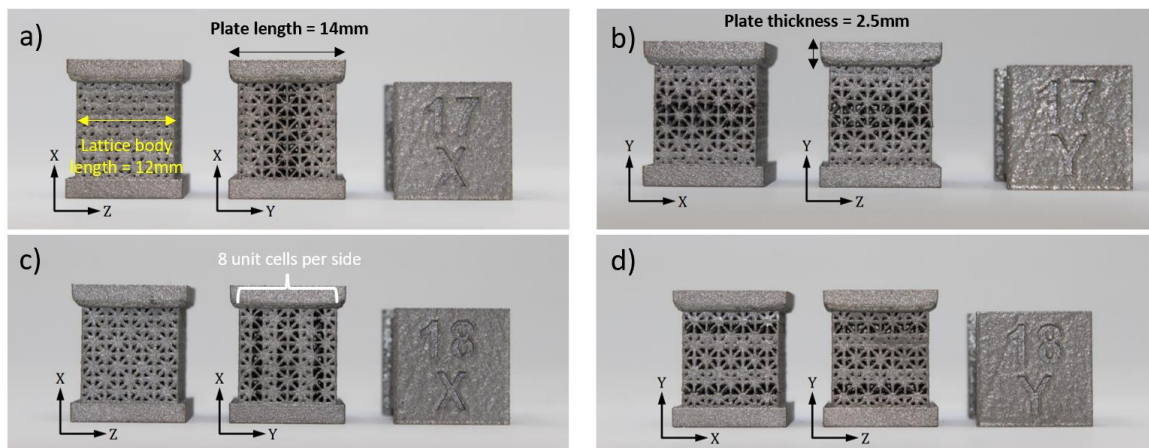

Fig. 3. All 12 compression samples shown. Each sample group shows the front, side, and top view. For clarity, dimensions are distributed in different photos, but all the samples are manufactured to the same size. a) x-direction type L, b) y-direction type L, c) x-direction type S, and d) y-direction type S

Micro-CT Imaging

Micro-computed Tomography (micro-CT) imaging of 3D-printed lattice structures was used for evaluating the effect of grading on printed strut sizes. Cross-sectional areas of both uniform and graded struts, located at the transition between cells with different densities, were measured from the reconstructed micro-CT slices. A Bruker SkyScan 1272 micro-CT scanner (maximum 100 μA and 100 kV) was used in this study. Due to the limited X-ray power of the available desktop micro-CT scanner model and limited field of view, micro-CT specific samples were designed on a 4-by-4-by-4 grid using the same building block unit cells with side lengths of 1.5, making them compact enough to fit inside the field of view of the scanner. A solid plate with width of 8 mm and thicknesses of 2 mm was added at the bottom of each lattice design for marking and easy mounting onto the micro-CT platform.

A total of five micro-CT samples were designed and manufactured, including four samples of uniform strut diameters ranging from 300 micron to 600 micron with an interval of 100 micron (**Fig. 4a**). An additional sample was designed such that it included transitions between unit cells of varying sizes, ranging from 100 microns for smoother transitions to 300 microns for sharper transitions (**Fig. 4b, 4c**). During scanning, the samples were placed and fixed on a rotating platform using clay. Due to the different solid volume fractions, exposure times ranged from 2500 milliseconds to 3500 milliseconds. All scans used a 0.11mm Cu filter to reduce noise. After scanning, the companion software for CT reconstruction was used to convert vertical X-ray images into horizontal slices. During this process, typical micro-CT post-processing correction methods such as alignment correction

and ring artifacts reduction were applied. The processed horizontal slices were then rebuilt into 3-D bodies using the marching cube algorithm [27] in the form of STL files with the same pixel size as used for CT reconstruction. Geomagic Wrap 2017 (*3D Systems*) was then used to register the reconstructed geometries from micro-CT to the designed lattice structures, and the relevant affine transformation (i.e., rotation matrix) for perfect alignment of imaged models was extracted. With the rotation matrices, the original 3-D bodies produced by the marching cube algorithm could be corrected to the right orientation and stored in the form of 3-D volumes in MATLAB.
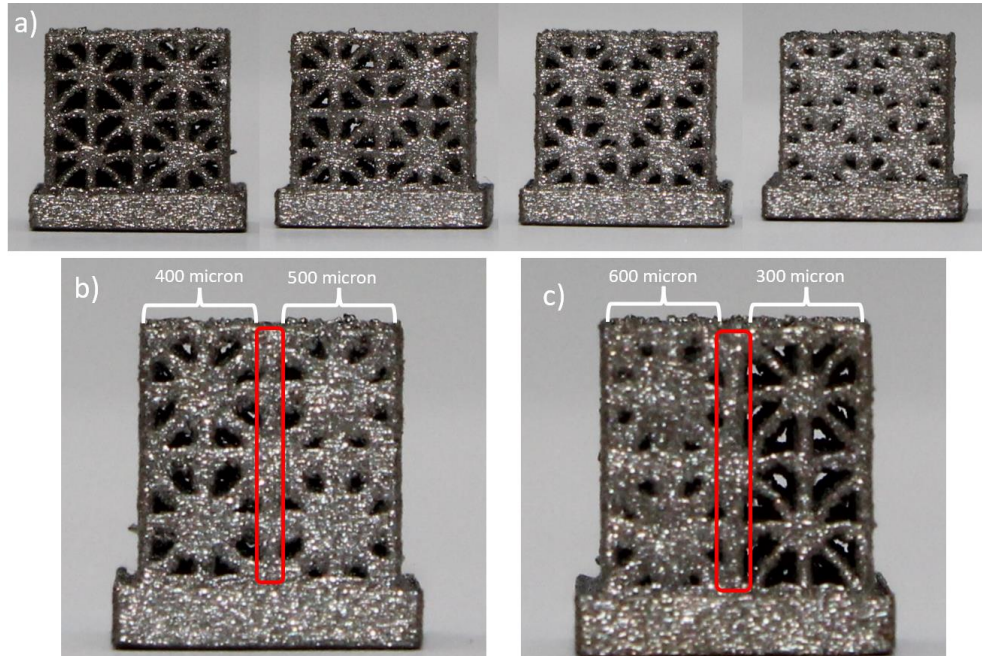

Fig. 4. a) Uniform strut thickness micro-CT samples from 300-600 micron with 100-micron interval. b) One side view of the graded micro-CT sample, with the center strut (marked in red) shared by the 400-micron and 500-micron side (linear grading). c) Another side view of the graded micro-CT sample, with the center strut shared by the 600-micron and 300-micron side (sharp grading).

A MATLAB script was developed for counting the number of solid pixels in binarized 2-D slices by sweeping along an axis of the stored 3-D volume. Slices in the vertical direction were used for measurements due to higher quality of images in Z-direction, which was the original axis of rotation during scanning. The cross-sectional area of struts were measured by finding the position of each strut and gradually expanding the upper and lower boundaries until the number of solid pixels dropped below a prescribed limit. At each expansion step, the algorithm computed the number of solid pixels that each boundary passed through within the width of the sample and compared against void pixels. To account for the surface roughness and compute the average thickness of the measured strut, each boundary stopped expanding until it passed through a target number of void pixels, which was defined as half of the theoretical number of solid pixels along that row if the sample were smooth. In this way, the thickness of the horizontal struts could be measured for each valid 2-D slice and integrated numerically for consecutive valid slices to compute the cross-sectional area of the strut. The benefit of computing the area rather than measuring only the maximum thickness was that it could account for the irregular cross-sectional shapes of the as-built struts, not assuming that the struts were all perfectly cylindrical when comparing the design and the as-built products, thus producing potentially more accurate results.

Results

Mechanical testing results

Force-displacement responses of three samples of each design, as obtained from the MTS measurements, generally match well over the entire loading range for all four cases (**Fig. 5**). It should be noted that technical difficulties with the video recording resulted in earlier stopping for tests on two samples of type L in Y-direction, thus displaying only a fraction of the entire compression testing compared to the other samples. However, since the tests interrupted after the yield point, the stiffness and yield strength could still be calculated for these samples. It is clear from the force-displacement curves that the mechanical responses of these lattice designs are different depending on the loading directions. However, the mechanical responses of sharply and smoothly graded lattices look similar in both loading directions. The processed stress-strain curves (**Fig. 6**) show that the overall trend in stiffness within each sample group is consistent, but some differences can still be observed. These differences may be attributed to manufacturing-induced defects which will be discussed in detail in micro-CT results. Samples loaded in Y-direction passed yielding at lower displacements than the X-direction samples, with the stress-strain curves becoming non-linear when the strain was around 1.5%, while X-direction samples did not yield until the strain reached at least 2.5% (**Table. 1**). The data labeled with subscript 1 represents the material properties of the entire sample including the top and bottom plates, and the data with subscript 2 represents the material properties of only the lattice part. These two sets of data combined represent the upper and lower estimations of the stiffness based on displacements recorded by MTS.
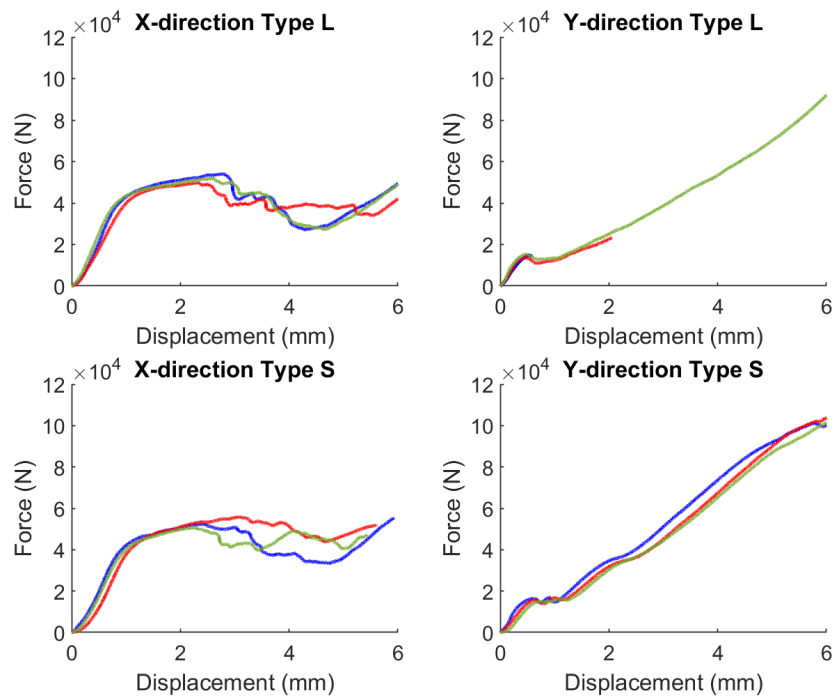
Fig. 5. Unprocessed force-displacement data directly from MTS (unit conversion from inch to mm is done).
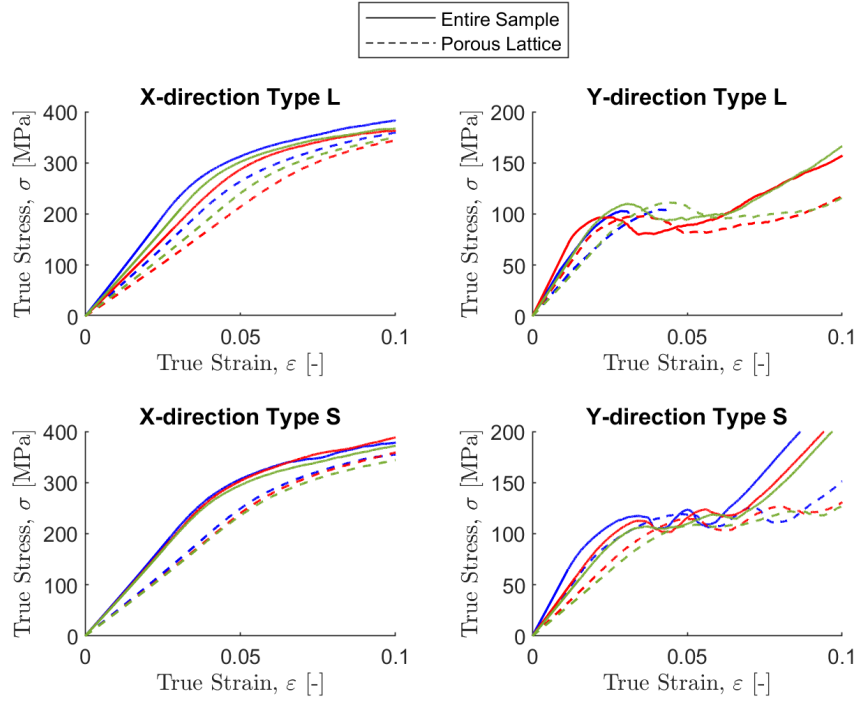
Fig. 6. True stress-strain curves for all samples processed from raw MTS data. Solid lines represent the entire compression samples including the top and bottom plates, dashed lines represent only the lattice parts.

Table. 1. Effective material properties, i.e., elastic stiffness (E_t), yield stress (σ_Y) and yield strain (ε_Y) of test samples as obtained from MTS data $(\cdot)_1$, $(\cdot)_2$ and DIC-adjusted data $(\cdot)_{DIC}$.

| Sample Group	Sample Number	$E_{t,1}$ [GPa]	$E_{t,2}$ [GPa]	$E_{t,DIC}$ [GPa]	$\sigma_{Y,1}$ [MPa]	$\sigma_{Y,2}$ [MPa]	$\sigma_{Y,DIC}$ [MPa]	$\varepsilon_{Y,1}$ [-]	$\varepsilon_{Y,2}$ [-]	$\varepsilon_{Y,DIC}$ [-]
Type L (X-dir)	1	7.66	5.30	6.84	275.5	282.9	281.4	0.039	0.056	0.043
	2	5.82	4.03	4.48	297.4	312.5	307.1	0.053	0.079	0.066
	3	6.56	4.53	7.14	290.8	301.1	282.8	0.046	0.068	0.041
Average (SD)		6.68 (0.92)	4.618 (0.64)	6.15 (1.46)	287.9 (14.9)	298.9 (14.9)	290.4 (14.4)	0.046 (0.0071)	0.068 (0.011)	0.050 (0.014)
Type L (Y-dir)	1	4.99	3.45	3.85	81.9	77.7	81.0	0.0184	0.0245	0.0230
	2	6.05	4.18	4.46	88.4	87.5	89.8	0.016	0.022	0.022
	3	4.56	3.19	3.80	101.1	100.1	97.9	0.024	0.033	0.027
Average (SD)		5.21 (0.76)	3.61 (0.50)	4.04 (0.36)	90.4 (9.7)	88.4 (11.1)	89.6 (8.4)	0.019 (0.004)	0.027 (0.0056)	0.024 (0.0031)
Type S (X-dir)	1	6.80	4.76	5.72	288.6	297.9	290.4	0.044	0.064	0.052
	2	6.57	4.54	5.35	291.1	301.8	297.6	0.046	0.068	0.057
	3	6.48	4.48	5.23	280.0	289.5	285.6	0.045	0.066	0.056
Average (SD)		6.62 (0.16)	4.60 (0.14)	5.43 (0.25)	286.5 (5.8)	296.4 (6.3)	291.2 (6.0)	0.045 (0.0009)	0.066 (0.0019)	0.055 (0.0025)
Type S (Y-dir)	1	5.57	3.89	4.59	92.9	91.4	88.7	0.018	0.025	0.021
	2	4.04	2.79	3.16	102.1	102.2	103.2	0.027	0.038	0.034
	3	3.58	2.47	3.54	100.3	101.2	78.5	0.030	0.042	0.024
Average (SD)		4.40 (1.04)	3.06 (0.74)	3.76 (0.74)	98.5 (4.8)	98.3 (5.9)	90.1 (12.4)	0.025 (0.0059)	0.035 (0.009)	0.026 (0.007)

DIC was able to track pixel patterns and output both horizontal and vertical displacements and surface strains (not shown here) successfully. By incorporating DIC, the adjusted force-displacement data was used to calculate stiffness, yield strength and yield strain (**Fig. 7**). Note that since DIC only tracks the deformation of the lattice parts, DIC adjusted data only applies to the lattice part, excluding the top and bottom plates.

| Time (sec)	Horizontal Displacement (u_x)	Vertical Displacement (u_y)
0		
10		
20		
30		
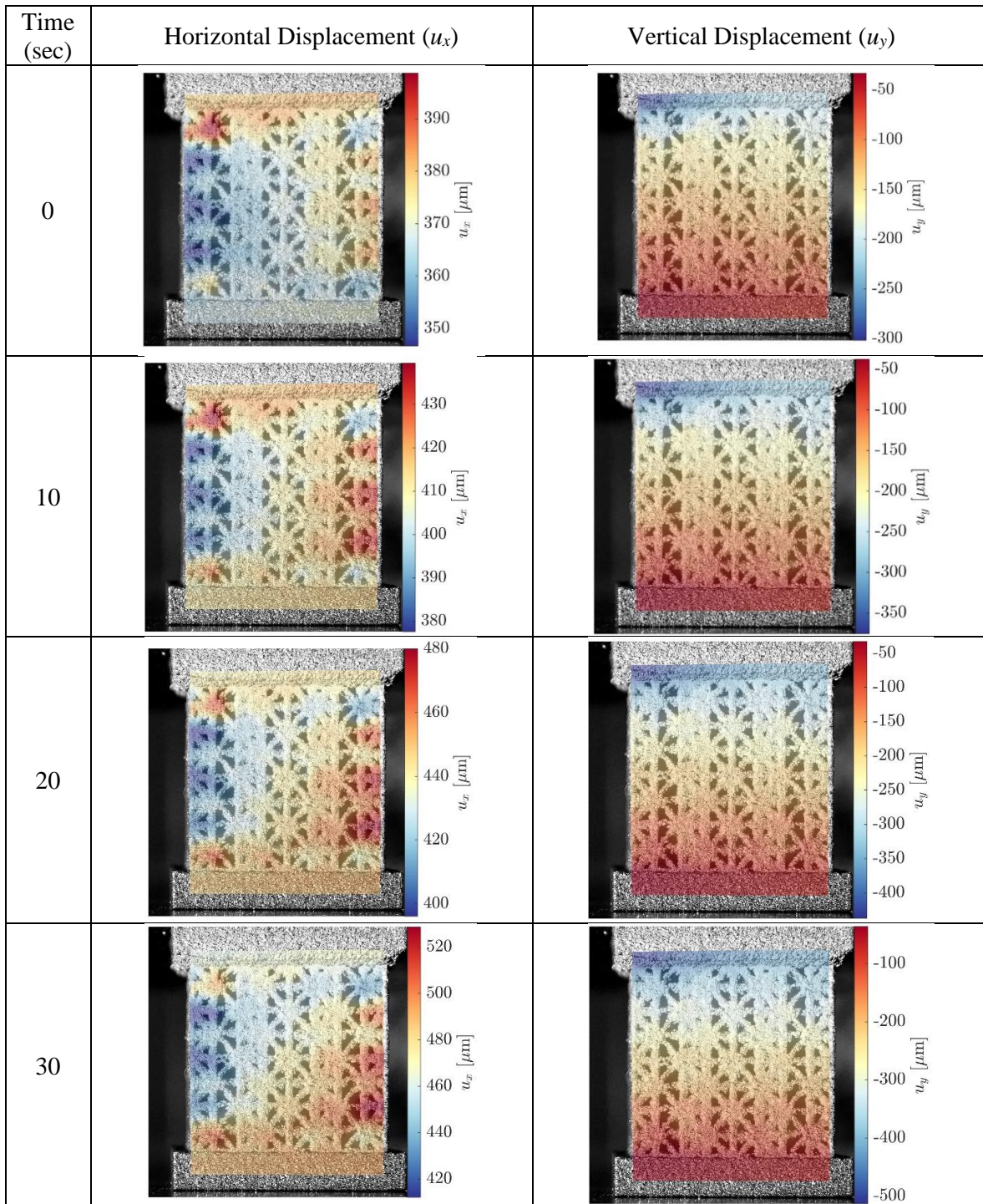
Fig. 7. DIC processing snapshots for horizontal and vertical displacement in a 30-second interval (X-direction type S sample shown).

The results show that for all samples, DIC adjusted stiffness and yield strength for porous lattice parts are larger than non-adjusted ones. Overall, the stress-strain responses computed from the DIC were comparable to those calculated from only the MTS measurements when averaging over three samples of each lattice design. The analysis of variations within each design showed that the stress-strain curves from the DIC generally would fall between those from MTS (**Fig. 8**). The standard deviation was calculated using the data points from three samples within each sample group throughout the range of DIC-processable displacement range. For the sample groups that have all three DIC processable videos, the displacement adjustment ratio from each video was applied to its corresponding sample individually. For the sample groups that have less than three suitable videos, adjustment factors for the samples without valid videos were estimated as an average from the available correction ratios within the same sample group. The average stiffness of type S samples are slightly smaller than type L samples in the same loading direction, but because of the rather substantial standard deviation, the differences are not large enough to produce statistical significance. There are also no statistically significant differences in yield stress and yield strain between type S and type L samples in the same loading direction. Anisotropy is clearly observed, particularly in yield stress for the same grading type loaded in different directions, as the X-direction type L and type S samples have yield stresses around 290 MPa, while both Y-direction samples are around 90 MPa. Although anisotropy is less pronounced in stiffness than yield stress, statistical significance still exists to support the observation. These findings are summarized in **Table. 1 and Fig 9**. The data labeled with subscript DIC represents the material properties calculated from the force data given by MTS and displacement data adjusted according to DIC results.
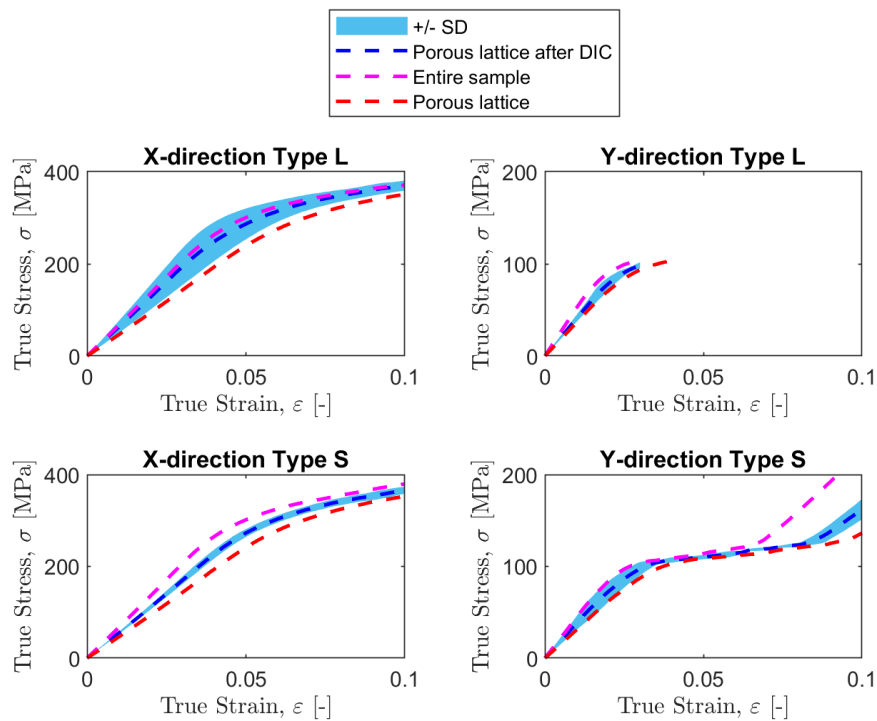

Fig. 8. Average raw true stress-strain curves and DIC processed stress-strain curves with +/- one standard deviation.
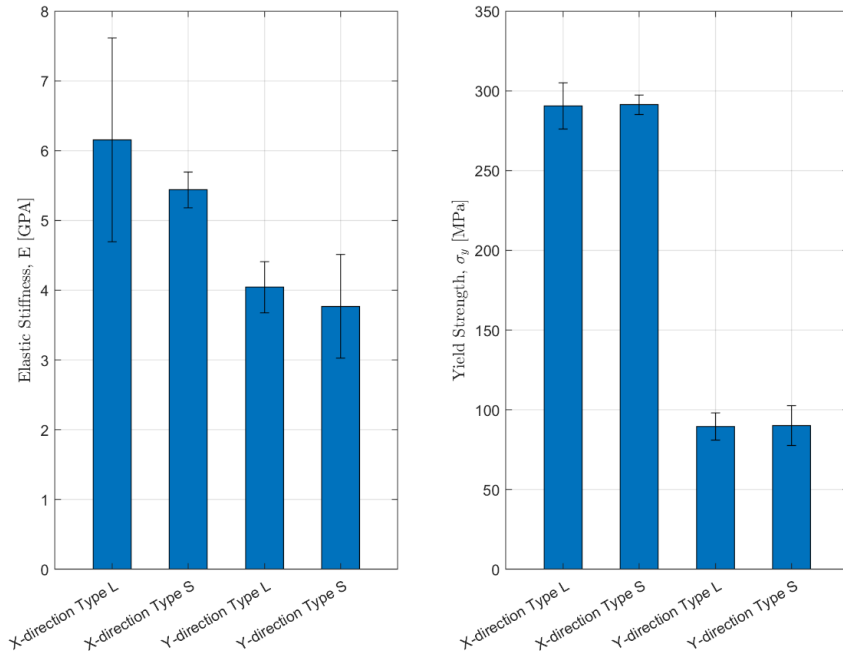
Fig. 9. Comparison of elastic stiffness and yield strength by sample group. Error bars show standard deviations.

Micro-CT results

Processing micro-CT scans revealed 25 to 40% increase in strut cross-sectional areas of as-built samples compared to original designs for uniform and type L designs, whereas the type S as-built sample only had an average of 13% increase, as is shown in **Fig. 10.** These differences in cross-sectional area are equivalent to 12 to 20% increase in strut widths for lattices with uniform density and type L grading, and 6% larger strut widths for sharply graded type S. The error bars represent the standard deviation and were calculated from the measurements of 9 struts per uniform design and 3 struts per graded design. The reason why graded designs have less available struts is that the graded struts were all integrated into one sample, while the uniform designs have a total of 4 samples for different strut diameters, thus providing more data. Manufacturing-induced defects were also observed in all samples **(Fig. 11).** The most common defect is manufacture-induced defective pores (marked in yellow circles), which were observed in all strut thicknesses. At lower volume fractions, manufacturing-induced disconnected struts (marked in red circles) started to appear, potentially due to the strut thicknesses approaching the minimum printing feature size (254 μm). At higher volume fractions, particularly the uniform 600-micron sample, designed void spaces (see as dark triangles in images) tended to lose geometric conformity, deforming from triangles into irregular shapes (marked in blue circles).
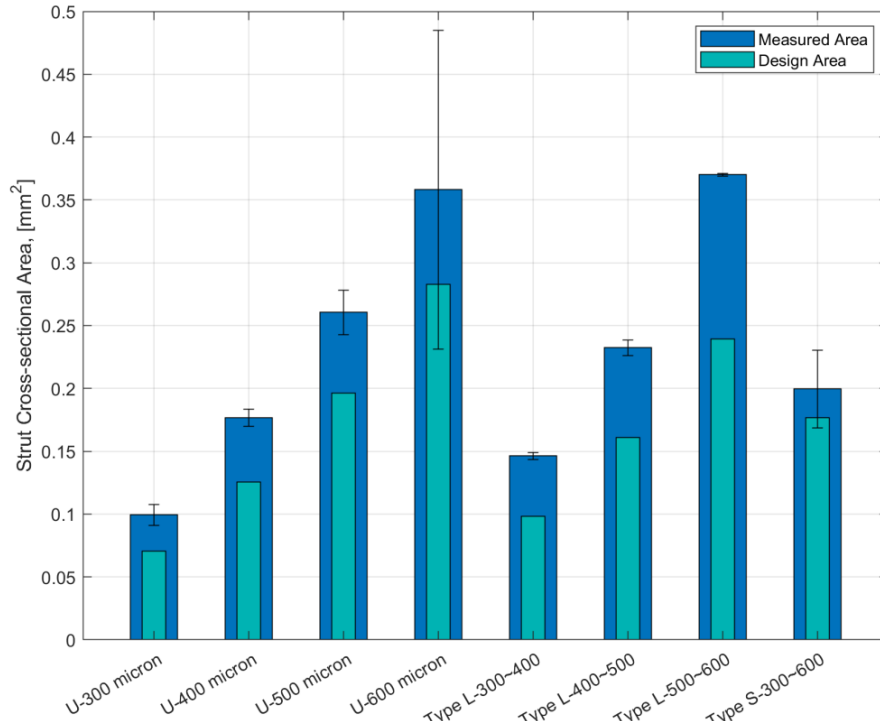
Fig. 10. Comparison of micro-CT measurements and original design. U: uniform samples. A~B: the strut that is shared in grading by the side with a thickness of A and another side of B.
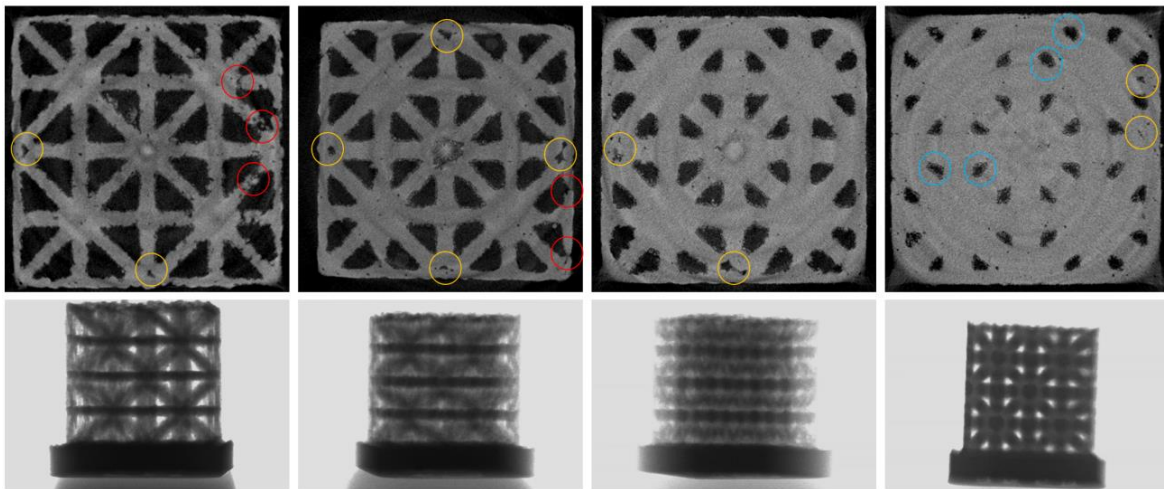
Fig. 11. Up: reconstructed micro-CT slices for uniform samples with manufacturing-induced defects. Down: X-ray images of corresponding samples.

Discussion

In this study, a total of 12 samples were compression tested and 5 samples were micro-CT scanned. It was found that with the same relative density, linearly graded (type L) and sharply graded (type S) lattices have no statistically significant difference in mechanical properties, such as stiffness and yield stress, when loaded in the same direction. The average value of stiffness for type S lattices were all slightly smaller than that of type L lattice, but the lack of statistical significance in the findings may be attributed to two reasons: the small sample size (n=3) and large variations within properties of 3D-printed samples from the same design, potentially due to

random printing defects, or that the mechanical property differences caused by grading are inherently insignificant due to the printing process causing stress concentration regardless of the severity of discontinuity. The results from this study does not support the hypothesis that sharp grading can cause the material properties to decrease significantly compared to less aggressive linear grading. The compression testing did however prove that with the same building block and relative density, anisotropy could be achieved by functional grading, which was supported by significantly different yield stresses for samples loaded in different directions. Manufacturing defects likely caused the differences within each sample group, where defective pores and disconnected struts altered the effective properties beyond the designed targets. The 300-micron struts were found to be the most vulnerable ones to become disjointed. Since all the compression samples included 300-micron building blocks, disconnected struts might have been present in most of them, causing the samples within each group to differ in mechanical behaviors.

Micro-CT measurements found that the cross-sectional area of horizontal struts in uniform and type L as-built samples were systematically bigger than designs, and the percentage increase in area decreases as the strut diameter increases, indicating the possibility of a fixed increase in strut width in each layer when being printed. This could be resulted from overhang structures and attached powders, as is commonly found in SLM manufactured lattices [28]. Another possibility is that since the deviation in measured diameters are in the same order of magnitude as the printing layer thickness, the minimum feature size may be approaching the minimum printing resolution of the SLM process (30 μm) that was used, causing the struts to have larger widths by about twice the printing resolution. The sharply graded struts were found to be significantly smaller in percentage increase in cross-sectional area, which may explain the smaller average values for stiffness and yield stress of type S compression testing samples compared to type L ones. Nonetheless, due to random manufacturing-induced stress concentrations, the weakest struts in the sharply graded samples may not be the graded struts. Thus, even if the struts were printed relatively undersized compared to the linearly graded samples, it is still reasonable for the two designs to have similar material properties, since the stiffness and yield strength are largely dependent on the weakest members.

The results from mechanical testing were consistent with what was found in previous studies with similar relative density [28][11][29]. When comparing the mechanical behaviors of graded lattices, Xiao and Song concluded that step-wise graded and continuously graded lattices had similar properties [13]. Note that the grading method that Xiao and Song used was not the conventional method of adjusting strut thickness but by changing the geometry of building blocks (i.e., changing the angles between struts to make nodes closer to each other, or aspect ratio grading). This method is less flexible in terms of tuning relative density compared to strut size-based density grading. The range of relative density achieved in their study was about 8.5% (=22.5%-14%) using rhombic dodecahedron unit cells, as opposed to 42% (=79%-37%) using the hierarchical lattice design method used in this study. Combining this study to what Xiao and Song found, and the fact that few experimental studies have achieved a statistical significance in material property differences when using different grading methods, it is speculated that when the relative density is constant, abrupt grading may not cause a significant loss of material properties, as opposed to what computational modeling suggests [30].

The reason why some samples within the same sample group behave differently is not completely understood. It may have been caused by manufacturing-induced defects, as is presented in micro-CT results and is also found by Timercan, Terriault and Brailovski [20]. Due to the size of compression samples, micro-CT scans are not possible with existing equipment because the samples exceed the dimension limits of the specimen chamber. Additionally, the cross-sectional areas of vertical and diagonal struts have not yet been studied. The SLM manufacturing process is known to produce different microstructure features induced by cooling rates during solidification when printing in different directions [31]. Finally, although the conclusion for micro-CT measurement is that sharply graded struts have a smaller increase in area compared to design than uniform and linearly graded struts, the exact reason in terms of printing parameters, laser movement and cooling is unknown, since the printer is not in-house.

Conclusion

The main goal of this work is to experimentally test hierarchical functionally graded lattices using Digital Image Correlation and micro-CT.

- Static compressive testing showed that the average elastic stiffness and yield strength of lattice structures with sharp grading (type S) is slightly smaller than type linearly graded (type L) samples, though no statistically significant results can be drawn, indicating that material properties may not have strong correlation with the severity of discontinuity in lattice structure due to discrete unit cell grading, given a fixed overall relative density.
- It was observed that anisotropy can be achieved through hierarchical material and functional grading. By tuning relative density at different locations of the lattice, functionally graded hierarchical building blocks can resemble Voigt's iso-strain and Reuss's iso-stress conditions successfully. Further potential in more accurately tuning anisotropy can be explored.

References

[1] Yang L, Li Y, Wu S, Chen P, Wu H, Su J, et al. Tailorable and predictable mechanical responses of additive manufactured TPMS lattices with graded structures. Materials Science and Engineering: A 2022;843:143109. https://doi.org/10.1016/j.msea.2022.143109.

[2] Zhou D, Gao Y, Lai M, Li H, Yuan B, Zhu M. Fabrication of NiTi Shape Memory Alloys with Graded Porosity to Imitate Human Long-bone Structure. J Bionic Eng 2015;12:575–82. https://doi.org/10.1016/S1672-6529(14)60147-5.

[3] Liao B, Xia RF, Li W, Lu D, Jin ZM. 3D-Printed Ti6Al4V Scaffolds with Graded Triply Periodic Minimal Surface Structure for Bone Tissue Engineering. J Mater Eng Perform 2021;30:4993–5004. https://doi.org/10.1007/s11665-021-05580-z.

[4] Rho J-Y, Roy ME, Tsui TY, Pharr GM. Elastic properties of microstructural components of human bone tissue as measured by nanoindentation. J Biomed Mater Res 1999;45:48–54. https://doi.org/10.1002/(SICI)1097-4636(199904)45:1<48::AID-JBM7>3.0.CO;2-5.

[5] van Grunsven W, Hernandez-Nava E, Reilly G, Goodall R. Fabrication and Mechanical Characterisation of Titanium Lattices with Graded Porosity. Metals (Basel) 2014;4:401–9. https://doi.org/10.3390/met4030401.

[6] Tan C, Zou J, Li S, Jamshidi P, Abena A, Forsey A, et al. Additive manufacturing of bio-inspired multi-scale hierarchically strengthened lattice structures. Int J Mach Tools Manuf 2021;167:103764. https://doi.org/10.1016/j.ijmachtools.2021.103764.

[7] Zhang XZ, Leary M, Tang HP, Song T, Qian M. Selective electron beam manufactured Ti-6Al-4V lattice structures for orthopedic implant applications: Current status and outstanding challenges. Curr Opin Solid State Mater Sci 2018;22:75–99. https://doi.org/10.1016/j.cossms.2018.05.002.

[8] Izri Z, Bijanzad A, Torabnia S, Lazoglu I. In silico evaluation of lattice designs for additively manufactured total hip implants. Comput Biol Med 2022;144:105353. https://doi.org/10.1016/j.compbiomed.2022.105353.

[9] Ren B, Wan Y, Liu C, Wang H, Yu M, Zhang X, et al. Improved osseointegration of 3D printed Ti-6Al-4V implant with a hierarchical micro/nano surface topography: An in vitro and in vivo study. Materials Science and Engineering: C 2021;118:111505. https://doi.org/10.1016/j.msec.2020.111505.

[10] Lin Y, Shi W, Li J, Liu Y, Liu S, Li J. Evaluation of mechanical properties of Ti–6Al–4V BCC lattice structure with different density gradient variations prepared by L-PBF. Materials Science and Engineering: A 2023;872:144986. https://doi.org/10.1016/j.msea.2023.144986.

[11] Wally ZJ, Haque AM, Feteira A, Claeyssens F, Goodall R, Reilly GC. Selective laser melting processed Ti6Al4V lattices with graded porosities for dental applications. J Mech Behav Biomed Mater 2019;90:20–9. https://doi.org/10.1016/j.jmbbm.2018.08.047.

[12] Yang L, Wu S, Yan C, Chen P, Zhang L, Han C, et al. Fatigue properties of Ti-6Al-4V Gyroid graded lattice structures fabricated by laser powder bed fusion with lateral loading. Addit Manuf 2021;46:102214. https://doi.org/10.1016/j.addma.2021.102214.

[13] Xiao L, Song W. Additively-manufactured functionally graded Ti-6Al-4V lattice structures with high strength under static and dynamic loading: Experiments. Int J Impact Eng 2018;111:255–72. https://doi.org/10.1016/j.ijimpeng.2017.09.018.

[14] Mahmoud D, Al-Rubaie KS, Elbestawi MA. The influence of selective laser melting defects on the fatigue properties of Ti6Al4V porosity graded gyroids for bone implants. Int J Mech Sci 2021;193:106180. https://doi.org/10.1016/j.ijmecsci.2020.106180.

[15] Soro N, Saintier N, Merzeau J, Veidt M, Dargusch MS. Quasi-static and fatigue properties of graded Ti–6Al–4V lattices produced by Laser Powder Bed Fusion (LPBF). Addit Manuf 2021;37:101653. https://doi.org/10.1016/j.addma.2020.101653.

[16] Onal E, Frith JE, Jurg M, Wu X, Molotnikov A. Mechanical properties and in vitro behavior of additively manufactured and functionally graded Ti6Al4V porous scaffolds. Metals (Basel) 2018;8. https://doi.org/10.3390/met8040200.

[17] Salem H, Carter LN, Attallah MM, Salem HG. Influence of processing parameters on internal porosity and types of defects formed in Ti6Al4V lattice structure fabricated by selective laser melting. Materials Science and Engineering: A 2019;767:138387. https://doi.org/10.1016/j.msea.2019.138387.

[18] De Biasi R, Murchio S, Sbettega E, Carmignato S, Luchin V, Benedetti M. Efficient optimization framework for L-PBF fatigue enhanced Ti6Al4V lattice component. Mater Des 2023;230:111975. https://doi.org/10.1016/j.matdes.2023.111975.

[19] Kas M, Yilmaz O. Radially graded porous structure design for laser powder bed fusion additive manufacturing of Ti-6Al-4V alloy. J Mater Process Technol 2021;296:117186. https://doi.org/10.1016/j.jmatprotec.2021.117186.

[20] Timercan A, Terriault P, Brailovski V. Axial tension/compression and torsional loading of diamond and gyroid lattice structures for biomedical implants: Simulation and experiment. Mater Des 2023;225. https://doi.org/10.1016/j.matdes.2022.111585.

[21] Dallago M, Zanini F, Carmignato S, Pasini D, Benedetti M. Effect of the geometrical defectiveness on the mechanical properties of SLM biomedical Ti6Al4V lattices. Procedia Structural Integrity, vol. 13, Elsevier B.V.; 2018, p. 161–7. https://doi.org/10.1016/j.prostr.2018.12.027.

[22] Shi J, Akbarzadeh AH. 3D Hierarchical lattice ferroelectric metamaterials. Int J Eng Sci 2020;149. https://doi.org/10.1016/j.ijengsci.2020.103247.

[23] Al-Saedi DSJ, Masood SH, Faizan-Ur-Rab M, Alomarah A, Ponnusamy P. Mechanical properties and energy absorption capability of functionally graded F2BCC lattice fabricated by SLM. Mater Des 2018;144:32–44. https://doi.org/10.1016/j.matdes.2018.01.059.

[24] Plocher J, Panesar A. Mechanical Performance of Additively Manufactured Fiber-Reinforced Functionally Graded Lattices. JOM 2020;72:1292–8. https://doi.org/10.1007/s11837-019-03961-3.

[25] Zhang X-Y, Fang G, Xing L-L, Liu W, Zhou J. Effect of porosity variation strategy on the performance of functionally graded Ti-6Al-4V scaffolds for bone tissue engineering. Mater Des 2018;157:523–38. https://doi.org/10.1016/j.matdes.2018.07.064.

[26] Yang J, Bhattacharya K. Augmented Lagrangian Digital Image Correlation. Exp Mech 2019;59:187–205. https://doi.org/10.1007/s11340-018-00457-0.

[27] Peter Hammer. Marching Cubes. MATLAB Central File Exchange 2023. https://www.mathworks.com/matlabcentral/fileexchange/32506-marching-cubes (accessed September 9, 2023).

[28] Xu Y, Huang G, Li T, Tan Y, Bao T. Compressive properties of Ti6Al4V Functionally Graded Lattice Structures via topology optimization design and selective laser melting fabrication. Materials Science and Engineering A 2022;860. https://doi.org/10.1016/j.msea.2022.144265.

[29] Zhu L, Wang X, Sun L, Hu Q, Li N. Optimisation of Selective Laser Melted Ti6Al4V Functionally Graded Lattice Structures Accounting for Structural Safety. Materials 2022;15. https://doi.org/10.3390/ma15249072.

[30] Baldwin M, Meisel NA, Mccomb C. A Data-Driven Approach for Multi-Lattice Transitions. n.d.

[31]   Pilgar CM, Fernandez AM, Lucarini S, Segurado J. Effect of printing direction and thickness on the mechanical behavior of SLM fabricated Hastelloy-X. Int J Plast 2022;153. https://doi.org/10.1016/j.ijplas.2022.103250.